

Nowcasting transmission and suppression of the Delta variant of SARS-CoV-2 in Australia

Sheryl L. Chang¹, Oliver M. Cliff^{1,2}, Cameron Zachreson^{1,3}, Mikhail Prokopenko^{1,4}

¹ Centre for Complex Systems, Faculty of Engineering, The University of Sydney, Sydney, NSW 2006, Australia

² School of Physics, The University of Sydney, Sydney, NSW 2006, Australia

³ School of Computing and Information Systems, The University of Melbourne, Parkville, VIC 3052, Australia

⁴ Sydney Institute for Infectious Diseases, The University of Sydney, Westmead, NSW 2145, Australia

Correspondence to:

Prof Mikhail Prokopenko, Centre for Complex Systems
Faculty of Engineering, University of Sydney, Sydney, NSW 2006, Australia
mikhail.prokopenko@sydney.edu.au

Summary

As of July 2021, there is a continuing outbreak of the B.1.617.2 (Delta) variant of SARS-CoV-2 in Sydney, Australia. The outbreak is of major concern as the Delta variant is estimated to have twice the reproductive number of previous variants that circulated in Australia in 2020, which is worsened by low levels of acquired immunity in the population. Using a re-calibrated agent-based model, we explored a feasible range of non-pharmaceutical interventions, in terms of both mitigation (case isolation, home quarantine) and suppression (school closures, social distancing). Our nowcasting modelling indicates that the level of social distancing currently attained in Sydney is inadequate for the outbreak control. A counter-factual analysis suggests that if 80% of agents comply with social distancing, then at least a month is needed for the new daily cases to reduce from their peak to below ten. A small reduction in social distancing compliance to 70% lengthens this period to 45 days.

Introduction

Strict mitigation and suppression measures eliminated local transmission of SARS-CoV-2 during the initial pandemic wave in Australia (March–June 2020)¹, as well as a second wave that developed in the South Eastern state of Victoria (June–September 2020)^{2,3}. Several subsequent outbreaks were also detected and managed quickly and efficiently by contact tracing and local lockdowns, e.g., a cluster in the Northern Beaches Council of Sydney, New South Wales (NSW) totalled 217 cases and was controlled in 32 days by locking down only the immediately affected suburbs (December 2020–January 2021)⁴. Overall, the successful pandemic response was ensured by effective travel restrictions and social distancing, underpinned by comprehensive disease surveillance^{5,6,7,8,9}.

Unfortunately, the situation changed in mid-June 2021, when a highly transmissible variant of concern, B.1.617.2 (Delta), was detected. The first infection was recorded on June 16 in Sydney, and quickly spread through the Greater Sydney area. Within ten days, there were more than 100 locally acquired cumulative cases, triggering social distancing restrictions imposed in Greater Sydney and nearby areas¹⁰. By July 9 (23 days later), the locally acquired cases totalled 439⁴, and a tighter lockdown was announced¹⁰. Further restrictions and business shut-downs, including construction and retail industries, were announced on 17 July¹¹. The risk of a prolonged lockdown has become apparent¹², with no peak in incidence or prevalence confirmed at the time of writing.

The difficulty of controlling the outbreak is attributed to the high transmissibility of the B.1.617.2 (Delta) variant, which is known to increase the risk of household transmission by approximately 60% in comparison to the B.1.1.7 (Alpha) variant¹³. This transmissibility is compounded by the low rate of vaccination in

Australia, with around 6% of the population fully vaccinated before the Sydney outbreak and only 7.92% of Australians fully vaccinated by the end of June 2021¹⁴, with this fraction increasing to 15.87% by 24 July 2021¹⁵.

Several additional factors make the Sydney outbreak an important case study. Since previous pandemic waves were eliminated in Australia, the Delta variant has not been competing with other variants. This allows us to estimate its basic reproduction number, R_0 , in a cleaner setting. This transparency is further strengthened by low levels of acquired immunity to SARS-CoV-2 in the Australian population, given: (a) the pre-existing natural immunity is limited by cumulative confirmed cases of around 0.12%, and (b) immunity acquired due to vaccination is limited by vaccination coverage. Furthermore, the school winter break in NSW (28 June – 9 July) coincided with the period of social distancing restrictions announced on 26 June, with school premises remaining mostly closed beyond 9 July. Thus, the epidemic suppression policy of school closures is not a free variable, reducing the search space of available control measures.

This study addresses several important questions. Firstly, we calibrate reproductive number, R_0 , and generation period, T_{gen} , of the Delta variant, using real-world data for an ongoing outbreak in Australia, in a transparent epidemiological setting. Secondly, in a nowcasting mode, we investigate a feasible range of key non-pharmaceutical interventions (NPIs): case isolation, home quarantine, school closures and social distancing, available to control the virus transmission within the population with a low acquired immunity. Finally, in a counter-factual mode, we quantify under what conditions the ongoing outbreak can be suppressed, aiming to provide actionable information on the extent of required NPIs (concurrent with an accelerating vaccination rollout), in comparison to previous pandemic control measures successfully deployed in Australia.

Methods

We utilised an agent-based model (ABM) for transmission and control of COVID-19 in Australia that has been developed in our previous work^{1,16} and implemented within a large-scale software simulator (AMTraC-19). The model was cross-validated with genomic surveillance data⁵, and contributed to social distancing policy recommendations broadly adopted by the World Health Organisation¹⁷. The model separately simulates each individual as an agent within a surrogate population composed of about 23.4 million software agents. These agents are stochastically generated to match attributes of anonymous individuals (in terms of age, residence, gender, workplace, susceptibility and immunity to diseases), informed by data from the Australian Census and the Australian Curriculum, Assessment and Reporting Authority. In addition, the simulator follows the known commuting patterns between the places of residence and work/study^{18,19,20}. Different contact rates specified within diverse social contexts (e.g., households, neighbourhoods, communities, and work/study environments) explicitly represent heterogeneous demographic and epidemic conditions. The model has previously been calibrated to produce characteristics of the COVID-19 pandemic corresponding to the ancestral lineage of SARS-CoV-2^{1,16}, using actual data from the first and second waves in Australia, and re-calibrated for B.1.617.2 (Delta) variant using incidence data of the Sydney outbreak (see Supplementary Material: Model calibration).

Each epidemic scenario is simulated by updating agents' states in discrete time. In this work we start from an initial distribution of infection, seeded by imported cases generated by the incoming international air traffic in Sydney's international airport (using data from the Australian Bureau of Infrastructure, Transport and Regional Economics)^{18,19}. At each time step during the seeding phase, this process probabilistically generates new infections within a 50 km radius of the airport, in proportion to the average daily number of incoming passengers (using a binomial distribution and data from the Australian Bureau of Infrastructure, Transport and Regional Economics)¹⁸.

A specific outbreak, originated in proximity to the airport, is traced over time by simulating the agents interactions within their social contexts, computed in 12-hour cycles ("day" and "night"). Once the outbreak size (cumulative incidence) exceeds a pre-defined threshold (e.g., 20 detected cases), the travel restrictions (TR) are imposed by the scenario, so that the rest of infections are driven by purely local transmissions, while no more overseas acquired cases are allowed (presumed to be in effective quarantine). Case-targeted non-pharmaceutical interventions (CTNPIs), such as case isolation (CI) and home quarantine (HQ), are

applied from the outset. A scenario develops under some partial mass-vaccination coverage, implemented as either a progressive rollout, or a limited pre-pandemic phase, as described in Supplementary Material: Vaccination modelling.

The outbreak-growth phase can then be interrupted by another, “suppression”, threshold (e.g., 100 or 400 cumulative detected cases) which triggers a set of general NPIs, such as social distancing (SD) and school closures (SC). Every intervention is specified via a macro-distancing level of compliance (i.e., $SD = 0.8$ means 80% of agents are socially distancing), and a set of micro-distancing parameters that indicate the level of social distancing within a specific social context (households, communities, workplaces, etc.). For instance, for those agents that are compliant, contacts (and thus likelihood of infection) can be reduced during a lockdown to $SD_w = 0.1$ within workplaces and $SD_c = 0.25$ within communities, whilst maintaining contacts $SD_h = 1.0$ within households.

Results

In order to model transmission of B.1.617.2 (Delta) variant during the Sydney outbreak of COVID-19 (June–July 2021), we re-calibrated the model to obtain the reproduction number approximately twice as high as our previous estimates ($R_0 \approx 3.0$) for the two waves in Australia in 2020. In aiming at this level, we followed global estimates, which showed that the R_0 for B.1.617.2 is increased by 97% (95% CI of 76–117%) relative to its ancestral lineage²¹. The re-calibrated reproductive number was estimated to be $R_0 = 5.97$ with a 95% CI of 5.93–6.00. The corresponding generation period is estimated to be $T_{gen} = 6.88$ days with a 95% CI of 6.81–6.94 days. Supplementary Material describes sensitivity analysis of the model.

Using the ABM calibrated to the B.1.617.2 (Delta) variant, we varied the macro- and micro-parameters (for CI, HQ, SC and SD), aiming to match the incidence data recorded during the Sydney outbreak in a *nowcasting* mode. Within the considered timeline, a peak in the actual incidence time series is not observed; however, the actual incidence growth rate has reduced from $\beta_I = 0.098$ (17 June – 13 July), to $\beta_{II} = 0.076$ (17 June – 25 July), to $\beta_{III} = 0.037$ (16–25 July), as detailed in Supplementary Material: Growth rates. As shown in Fig. 1, the nowcasting horizon was set to July 25 and assumed a progressive vaccination rollout in addition to a tighter lockdown being imposed at 400 cases (corresponding to July 9).

The closest match to the actual incidence data over the entire period was produced by a moderate macro-level of social distancing compliance, $SD = 0.5$, or even a lower level ($SD = 0.4$) for the period up to 13 July (see Supplementary Material: Sensitivity of nowcasting outcomes, Fig. S2). Importantly, however, the growth in actual incidence during the period of the comprehensive lockdown restrictions (16–25 July) is best matched by a higher compliance level, $SD = 0.6$. This match is also reflected by proximity of the corresponding growth rate $\beta_{0.6} = 0.029$ to the incidence growth rate $\beta_{III} = 0.037$. The considered SD levels were based on moderately reduced interaction strengths within community, i.e., $SD_c = 0.25$, see Table 1, which were inadequate for the outbreak suppression even with high macro-distancing such as $SD = 0.7$.

Furthermore, we considered feasible macro-levels of social distancing, $0.5 \leq SD \leq 0.9$, while maintaining $CI = 0.7$ and $HQ = 0.5$, in a *counter-factual* mode by reducing the micro-parameters (the interaction strengths for CI, HQ, SC and SD) within their feasible bounds. Again, the control measures were triggered by cumulative incidence exceeding 400 cases (corresponding to a tighter lockdown imposed on July 9). An effective suppression of the outbreak within a reasonable timeframe is demonstrated for macro-distancing at $SD \geq 0.7$, coupled with the lowest feasible interaction strengths for most interventions, i.e., $NPI_c = 0.1$ (where NPI is one of CI, HQ, SC and SD), as shown in Fig. 2 and summarised in Table 1. For $SD = 0.8$, new cases reduce below 10 per day approximately a month (33 days) after the peak in incidence, while for $SD = 0.7$ this period reaches 45 days¹. Social distancing at $SD = 0.9$ is probably infeasible, but would reduce the new cases to below 10 a day within four weeks (25 days) following the peak in incidence.

Supplementary Material (Sensitivity of suppression outcomes) presents results obtained for the scenarios which assume a limited pre-pandemic vaccination phase (immunising 6% of the population). A positive impact of the partial progressive rollout which covers up to 40% of the population by mid-September is

¹A post-peak period duration for each SD level is obtained using the incidence trajectory averaged over ten simulation runs.

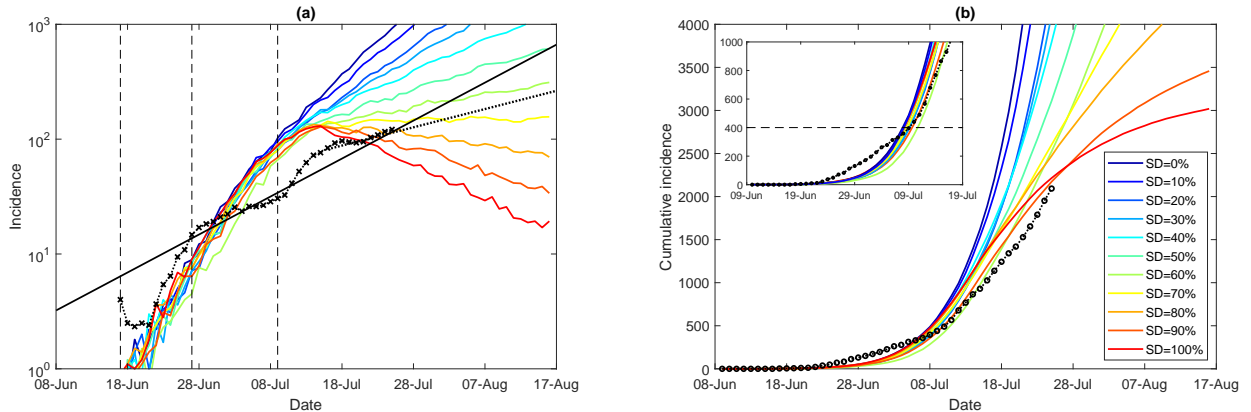


Figure 1: **Nowcasting up to July 25 (progressive vaccination rollout; suppression threshold: 400 cases): a comparison between actual epidemic curves and nowcasting simulation scenarios.** A moving average of the actual time series for (a) (log-scale) incidence (crosses), and (b) cumulative incidence (circles); with an exponential fit of the incidence’s moving average (black solid: β_{II} , and black dotted: β_{III}). Vertical dashed marks align the simulated days with the outbreak start (17 June, day 9), initial restrictions (27 June, day 19), and tighter lockdown (9 July, day 31). Traces corresponding to each social distancing (SD) compliance level are shown as average over 10 runs (coloured profiles for SD varying in increments of 10%, i.e., between $SD = 0.0$ and $SD = 1.0$). Each SD strategy, coupled with school closures, begins with the start of tighter lockdown, when cumulative incidence exceeds 400 cases (b: inset). The alignment between simulated days and actual dates may slightly differ across separate runs. Case isolation and home quarantine are in place from the outset.

Table 1: The macro-distancing parameters and interaction strengths: nowcasting (“now”) and counter-factual (“target”).

Strategy	Macro-distancing		Interaction strengths	
	Compliance levels now → target	Household	Community now → target	Workplace/School now → target
CI	0.7	1.0	0.25 → 0.1	0.25 → 0.1
HQ	0.5	2.0	0.25 → 0.1	0.25 → 0.1
SC (children)	1.0	1.0	0.5 → 0.1	0
SC (parents)	0.5	1.0	0.5 → 0.1	0
SD	0.4 → 0.8	1.0	0.25 → 0.1	0.1

counterbalanced by a delayed start of the tighter lockdown, with the 12-day delay leading to a higher peak-incidence, as can be seen by comparing Fig. 2 and Fig. S4. For example, for $SD = 0.8$, a scenario following the limited pre-pandemic vaccination, but imposing control measures earlier, demonstrates a reduction of incidence below 10 daily cases in four weeks (28 days) after the peak in incidence (Fig. S4), rather than 33 days under progressive rollout (Fig. 2). For $SD = 0.9$ the suppression periods differ by about one week: 17 days (Fig. S4) against 25 days (Fig. 2). However, this balance is nonlinear: for $SD = 0.7$, the suppression period under the pre-pandemic vaccination scenario approaches 55 days (Fig. S4), in contrast to the progressive rollout scenario achieving suppression earlier, in 45 days (Fig. 2). This is, of course, explained by the longer suppression period under $SD = 0.7$, during which a progressive rollout makes a stronger impact.

Discussion

Despite a relatively high computational cost, and the need to calibrate numerous internal parameters, ABMs capture the natural history of infectious diseases in a good agreement with the established estimates of incubation periods, serial/generation intervals, and other key epidemiological variables. Various ABMs

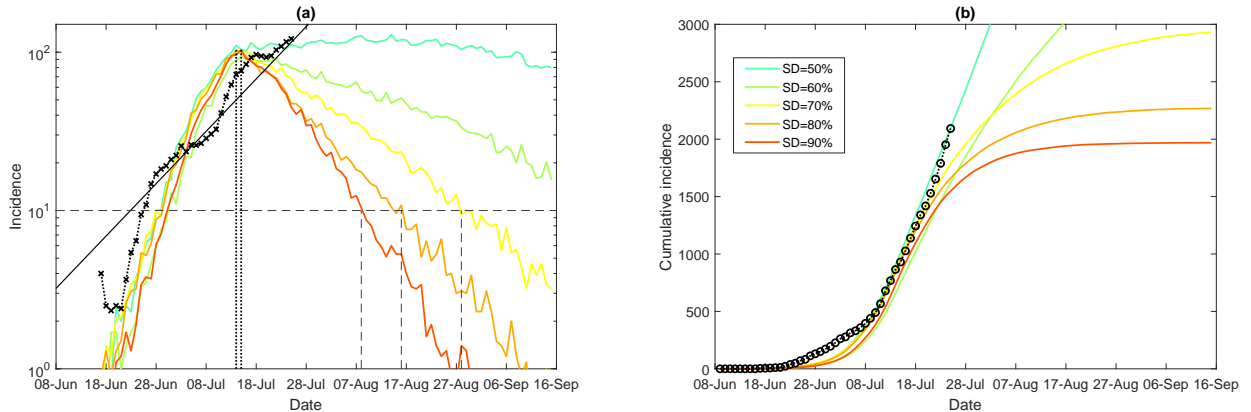


Figure 2: **Suppression after July 9 (progressive vaccination rollout; suppression threshold: 400 cases): a comparison between actual epidemic curves and counter-factual simulation scenarios.** A moving average of the actual time series for (a) (log scale) incidence (crosses), and (b) cumulative incidence (circles). Traces corresponding to feasible social distancing (SD) compliance levels are shown as average over 10 runs (coloured profiles for SD varying in increments of 10%, i.e., between $SD = 0.5$ and $SD = 0.9$). Vertical lines mark the incidence peaks (dotted) and reductions below 10 daily cases (dashed). Each SD strategy, coupled with school closures, begins with the start of tighter lockdown (i.e., July 9, simulated day 31), when cumulative incidence exceeds 400 cases. The alignment between simulated days and actual dates may slightly differ across separate runs. Case isolation and home quarantine are in place from the outset.

have been successfully used for simulating actual and counter-factual epidemic scenarios based on different initial conditions and intervention policies^{22,23,24,25}.

Our early COVID-19 study¹ modelled transmission of the ancestral lineage of SARS-CoV-2 characterised by the basic reproduction number of $R_0 \approx 3.0$ (adjusted $R_0 \approx 2.75$). This study compared several NPIs and identified the minimal SD levels required to control the first wave in Australia. Specifically, a compliance at the 90% level, i.e., $SD = 0.9$ (with $SD_w = 0$ and $SD_c = 0.5$) was shown to control the disease within 13-14 weeks. This relatively high SD compliance was required in addition to other restrictions (TR, CI, HQ), set at moderate levels of both macro-distancing ($CI = 0.7$ and $HQ = 0.5$), and interaction strengths: $CI_w = HQ_w = CI_c = HQ_c = 0.25$, $CI_h = 1.0$, and $HQ_h = 2.0$ ¹.

The follow-up work¹⁶ quantified possible effects of a mass-vaccination campaign in Australia, by varying the extents of *pre-pandemic* vaccination coverage with different vaccine efficacy combinations. This analysis considered hybrid vaccination scenarios using two vaccines adopted in Australia: BNT162b2 (Pfizer/BioNTech) and ChAdOx1 nCoV-19 (Oxford/AstraZeneca). Herd immunity was shown to be out of reach even when a large proportion (82%) of the Australian population is vaccinated under the hybrid approach, necessitating future partial NPIs for up to 40% of the population. The model was also calibrated to the basic reproduction number of the ancestral lineage ($R_0 \approx 3.0$, adjusted $R_0 \approx 2.75$), and used the same moderate interaction strengths as the initial study¹ (except $SD_c = 0.25$, reduced to match the second wave in Melbourne in 2020).

In this work, we re-calibrated the ABM to incidence data from the ongoing Sydney outbreak driven by the Delta variant. The reproductive number was estimated to be at least twice as high ($R_0 = 5.97$) as the one previously estimated for pandemic waves in Australia. We then explored effects of available NPIs on the outbreak suppression, under a *progressive vaccination* scenario. The nowcasting modelling identified that the current epidemic curves, which continued to grow (as of July 25), can be closely matched by moderate social distancing coupled with moderate interaction strengths within community (SD in $[0.4, 0.5]$, $SD_c = 0.25$), as well as moderate compliance with case isolation ($CI = 0.7$, $CI_w = CI_c = 0.25$) and home quarantine ($HQ = 0.5$, $HQ_w = HQ_c = 0.25$). The estimate of compliance has improved to $SD \approx 0.6$ during the period of comprehensive lockdown measures, announced on July 17.

We note that the workers delivering essential services are exempt from lockdown restrictions. The fraction of the exempt population can be inferred conservatively as 4% (strictly essential)²⁶, more comprehensively

as approximately 19% (including health care and social assistance; public administration and safety; accommodation and food services; transport, postal and warehousing; electricity, gas, water and waste services; financial and insurance services), but can reach more significant levels, around 33%, if all construction, manufacturing, and trade (retail/wholesale) are included in addition²⁷. The latter, broad-range, case limits feasible social distancing levels to approximately $SD \approx 0.7$. However, even with these inclusions, there is a discrepancy between the level estimated by ABM (SD in $[0.4, 0.5]$) and the broad-range feasible level ($SD \approx 0.7$). This discrepancy would imply that approximately 20-25% of the population have not been consistently complying with the imposed restrictions, while 30-35% may have been engaged in services deemed broadly essential (other splits comprising 50-60% of the “non-distancing” population are possible as well).

The inferred levels of social distancing are supported by real-world mobility data²⁸. Specifically, when compared to baseline (i.e., the median value for the corresponding day of the week, during the five-week period 3 January – 6 February 2020), the reports for July 16 show 31% reduction of mobility at workplaces, and 37% reduction of mobility in retail and recreation settings, with concurrent 65% reduction of mobility on public transport. On July 21, the mobility reductions are reported as 43% (workplaces), 41% (retail and recreation), and 72% (public transport). The extent of the mobility reduction in workplaces, as well as retail and recreation, closely match the social distancing levels estimated by the model (approximately 40%). Importantly, the interactions within workplaces and community contribute to the disease transmission stronger than contacts in public transport, and hence, a larger reduction in public transport mobility (around 70%) does not fully compensate for the continuing activities in other settings.

Moderate levels of compliance (SD in $[0.4, 0.6]$) would be inadequate for suppression of even less transmissible coronavirus variants¹. The Delta variant demands a stronger compliance and a reduction in the scope of essential services (especially, in a setting with low acquired immunity). Specifically, our results indicate that an effective suppression within a reasonable timeframe can be demonstrated only for the highest feasible compliance with social distancing ($SD \geq 0.7$), supported by dramatically reduced interaction strengths within the community and work/study environments ($NPI_c = NPI_w = 0.1$). Thus, this challenging goal can be achieved only in a combination of government actions (e.g., inclusion of some services previously deemed essential under the lockdown restrictions, while providing appropriate financial support to the affected businesses and employees), and a stronger community engagement with the suppression effort.

Obviously, the challenges of suppressing emerging variants of concern can be somewhat alleviated by a growing vaccination uptake. However, in Australia, the vaccination rollout continues to be limited by various supply and logistics constraints. Furthermore, as our results demonstrate, a progressive vaccination rollout reaching up to 40% of the population is counter-balanced by a delayed introduction of the tighter control measures. This balance indicates that timely and decisive interventions (“snap lockdowns”) strongly contribute to shortening of suppression periods, while a comprehensive mass-vaccination rollout plays a crucial role over a longer term and should preferably be carried out in a pre-outbreak phase¹⁶.

While the model was not directly used to inform policy, it forms part of the information set available to health departments, and we hope that its policy relevance can contribute to rapid and comprehensive responses in jurisdictions within Australia and overseas. A failure in suppression of this growing outbreak, whether due to inadequate population compliance or a desire to maintain and restart socioeconomic activities, is likely to generate a substantial pandemic wave affecting the entire nation^{29,30,31}.

Study limitations

In modelling the progressive vaccination rollout, we assumed a constant weekly uptake rate of 3%, while currently the rollout is accelerating. The rate of progressive vaccination is expected to vary, being influenced by numerous factors, such as access to national stockpiles, dynamics of social behaviour, and changing medical advice. The adopted estimate approximates the uptake within acceptable bounds, with discrepancies not exceeding 2% of the population at any simulated timepoint in July.

Another limitation is that the surrogate ABM population which corresponds to the latest available Australian Census data from 2016 (23.4M individuals, with 4.45M in Sydney) is smaller than the current Australian population (25.8M, with 4.99M in Sydney). This discrepancy is offset, however, by the outbreak size (three orders of magnitude smaller than Sydney population).

Finally, the model does not directly represent in-hotel quarantine and in-hospital transmissions. Since the frontline professionals (health care and quarantine workers) were vaccinated in a priority phase carried out in Australia in early 2021, i.e., before the Sydney outbreak, this limitation has a minor effect. Overall, as the epidemiology of the Delta variant continues to be refined with more data becoming available, our results may benefit from a retrospective analysis.

Contributors

MP conceived and co-supervised the study and drafted the original Article. SLC and MP designed the computational experiments and re-calibrated the model. SLC carried out the computational experiments, verified the underlying data, and prepared all figures. All authors had full access to all the data in the study. All authors contributed to the editing of the Article, and read and approved the final Article.

Declaration of interests

We declare no competing interests.

Data sharing

No unique source code was developed for this project. The actual incidence data is available at: <https://www.covid19data.com.au/>. The ABM contact and transmission rates are detailed elsewhere^{1,18}.

Acknowledgments

This work was partially supported by the Australian Research Council grant DP200103005 (MP and SLC). Additionally, CZ is supported in part by National Health and Medical Research Council project grant (APP1165876). AMTraC-19 is registered under The University of Sydney’s invention disclosure CDIP Ref. 2020-018. We are thankful for support provided by High-Performance Computing (HPC) service (Artemis) at the University of Sydney.

References

- [1] Chang SL, Harding N, Zachreson C, Cliff OM, Prokopenko M. Modelling transmission and control of the COVID-19 pandemic in Australia. *Nature Communications*. 2020;11(1):1–13.
- [2] Blakely T, Thompson J, Carvalho N, Bablani L, Wilson N, Stevenson M. The probability of the 6-week lockdown in Victoria (commencing 9 July 2020) achieving elimination of community transmission of SARS-CoV-2. *Medical Journal of Australia*. 2020;213(8):349–351.
- [3] Zachreson C, Mitchell L, Lydeamore MJ, Rebuli N, Tomko M, Geard N. Risk mapping for COVID-19 outbreaks in Australia using mobility data. *Journal of the Royal Society Interface*. 2021;18(174):20200657.
- [4] COVID-19 in Australia; 2021. Accessed on 10 July 2021. <https://www.covid19data.com.au/>.
- [5] Rockett RJ, Arnott A, Lam C, Sadsad R, Timms V, Gray KA, et al. Revealing COVID-19 transmission by SARS-CoV-2 genome sequencing and agent based modelling. *Nature Medicine*. 2020;26:1398–1404.
- [6] Scott N, Palmer A, Delpont D, Abeysuriya R, Stuart R, Kerr CC, et al. Modelling the impact of reducing control measures on the COVID-19 pandemic in a low transmission setting. *Medical Journal of Australia*. 2020;214(2):79–83.
- [7] Milne GJ, Xie S, Poklepovich D, O’Halloran D, Yap M, Whyatt D. A modelling analysis of the effectiveness of second wave COVID-19 response strategies in Australia. *Scientific Reports*. 2021;11(1):1–10.
- [8] Lokuge K, Banks E, Davis S, Roberts L, Street T, O’Donovan D, et al. Exit strategies: optimising feasible surveillance for detection, elimination, and ongoing prevention of COVID-19 community transmission. *BMC Medicine*. 2021;19(1):1–14.
- [9] Wilson N, Baker MG, Blakely T, Eichner M. Estimating the impact of control measures to prevent outbreaks of COVID-19 associated with air travel into a COVID-19-free country. *Scientific Reports*. 2021;11(1):1–9.
- [10] Health Protection NSW. COVID-19 in NSW – up to 8pm 9 July 2021; 2021. Accessed on 10 July 2021. <https://www.health.nsw.gov.au/Infectious/covid-19/Pages/stats-nsw.aspx>.
- [11] Nguyen, Kevin (17 July 2021). Sweeping new lockdown restrictions announced as NSW records 111 new COVID cases. ABC News; 2021. Accessed on 17 July 2021. <https://www.abc.net.au/news/2021-07-17/nsw-records-111-covid-19-cases/100300492>.

- [12] Chrysanthos, Natassia (10 July 2021). ‘The length of this lockdown is up to each and every one of us’: Berejiklian. The Age; 2021. Accessed on 10 July 2021. <https://www.theage.com.au/national/australia-covid-news-live-sydney-braces-for-weeks-of-lockdown-pfizer-covid-19-vaccine-distribution-brought-forward-20210710-p588ig.html?post=p52gi7>.
- [13] Public Health England. Latest updates on SARS-CoV-2 variants detected in UK; 2021. Accessed on 11 June 2021. <https://web.archive.org/web/202106111115707/https://www.gov.uk/government/news/confirmed-cases-of-covid-19-variants-identified-in-uk>.
- [14] Australian Government, Department of Health. COVID-19 Vaccine Roll-out; 2021. Accessed on 1 July 2021. <https://www.health.gov.au/sites/default/files/documents/2021/07/covid-19-vaccine-rollout-update-1-july-2021.pdf>.
- [15] Australian Government, Department of Health. COVID-19 Vaccine Roll-out; 2021. Accessed on 25 July 2021. <https://www.health.gov.au/sites/default/files/documents/2021/07/covid-19-vaccine-rollout-update-24-july-2021.pdf>.
- [16] Zachreson C, Chang SL, Cliff OM, Prokopenko M. How will mass-vaccination change COVID-19 lockdown requirements in Australia? *The Lancet Regional Health – Western Pacific*. 2021:accepted; also: arXiv:2103.07061.
- [17] World Health Organization. Calibrating long-term non-pharmaceutical interventions for COVID-19: Principles and facilitation tools – Manila: WHO Regional Office for the Western Pacific; Strengthening the health systems response to COVID-19: Technical guidance # 2: Creating surge capacity for acute and intensive care, 6 April 2020 – Regional Office for Europe; 2020.
- [18] Cliff OM, Harding M, Piraveen M, Erten Y, Gambhir M, Prokopenko M. Investigating spatiotemporal dynamics and synchrony of influenza epidemics in Australia: an agent-based modelling approach. *Simulation Modelling Practice and Theory*. 2018;87:412–431.
- [19] Zachreson C, Fair KM, Cliff OM, Harding M, Piraveenan M, Prokopenko M. Urbanization affects peak timing, prevalence, and bimodality of influenza pandemics in Australia: results of a census-calibrated model. *Science Advances*. 2018;4:eaa5294.
- [20] Fair KM, Zachreson C, Prokopenko M. Creating a surrogate commuter network from Australian Bureau of Statistics census data. *Scientific Data*. 2019;6:150.
- [21] Campbell F, Archer B, Laurenson-Schafer H, Jinnai Y, Konings F, Batra N, et al. Increased transmissibility and global spread of SARS-CoV-2 variants of concern as at June 2021. *Eurosurveillance*. 2021;26(24):2100509.
- [22] Germann TC, Kadau K, Longini IM, Macken CA. Mitigation strategies for pandemic influenza in the United States. *Proceedings of the National Academy of Sciences*. 2006 Apr;103(15):5935–5940.
- [23] Ajelli M, Gonçalves B, Balcan D, Colizza V, Hu H, Ramasco JJ, et al. Comparing large-scale computational approaches to epidemic modeling: agent-based versus structured metapopulation models. *BMC Infectious Diseases*. 2010;10(1):1–13.
- [24] Nsoesie EO, Beckman RJ, Marathe MV. Sensitivity analysis of an individual-based model for simulation of influenza epidemics. *PLOS ONE*. 2012;7(10):0045414.
- [25] Zachreson C, Fair KM, Harding N, Prokopenko M. Interfering with influenza: nonlinear coupling of reactive and static mitigation strategies. *Journal of The Royal Society Interface*. 2020;17(165):20190728.
- [26] Wang W, Wu Q, Yang J, Dong K, Chen X, Bai X, et al. Global, regional, and national estimates of target population sizes for COVID-19 vaccination: descriptive study. *BMJ*. 2020;371.
- [27] Vandenbroek P. Snapshot of employment by industry, 2019; 2019. Accessed on 10 July 2021. https://www.aph.gov.au/About_Parliament/Parliamentary_Departments/Parliamentary_Library/FlagPost/2019/April/Employment-by-industry-2019.
- [28] Google. Community Mobility Reports; 2021. Accessed on 25 July 2021. <https://www.google.com/covid19/mobility/>.
- [29] Viana J, van Dorp CH, Nunes A, Gomes MC, van Boven M, Kretzschmar ME, et al. Controlling the pandemic during the SARS-CoV-2 vaccination rollout. *Nature Communications*. 2021;12(1):1–15.
- [30] Abeysuriya R, Goutzamanis S, Hellard M, Scott N. Burnet Institute COVASIM modelling – NSW outbreak, 12 July 2021; 2021. Accessed on 23 July 2021. https://burnet.edu.au/system/asset/file/4797/Burnet_Institute_modelling_-_NSW_outbreak_12_July_2021_-_FINAL.pdf.
- [31] Ouakrim DA, Wilson T, Bablani L, Andrabi H, Thompson J, Blakely T. How long till Sydney gets out of lockdown?; 2021. Accessed on 23 July 2021. <https://pursuit.unimelb.edu.au/articles/how-long-till-sydney-gets-out-of-lockdown>.
- [32] Efron B, Tibshirani RJ. An introduction to the bootstrap. vol. 57 of *Monographs on statistics and applied probability*. Chapman and Hall New York; 1994.
- [33] Ferretti L, Wymant C, Kendall M, Zhao L, Nurtay A, Abeler-Dörner L, et al. Quantifying SARS-CoV-2 transmission suggests epidemic control with digital contact tracing. *Science*. 2020;368(6491).
- [34] Wu JT, Leung K, Bushman M, Kishore N, Niehus R, de Salazar PM, et al. Estimating clinical severity of COVID-19 from the transmission dynamics in Wuhan, China. *Nature Medicine*. 2020;26(4):506–510.
- [35] Zhang M, Xiao J, Deng A, Zhang Y, Zhuang Y, Hu T, et al. Transmission Dynamics of an Outbreak of the COVID-19 Delta Variant B.1.617.2 – Guangdong Province, China, May–June 2021. *Chinese Center for Disease Control and Prevention*. 2021;3(27):584–586.
- [36] Centers for Disease Control and Prevention. Interim Guidance on Duration of Isolation and Precautions for Adults with COVID-19; 2020. <https://www.cdc.gov/coronavirus/2019-ncov/hcp/duration-isolation.html>.
- [37] Arons MM, Hatfield KM, Reddy SC, Kimball A, James A, Jacobs JR, et al. Presymptomatic SARS-CoV-2 infections and transmission in a skilled nursing facility. *New England Journal of Medicine*. 2020;382(22):2081–2090.
- [38] Wölfel R, Corman VM, Guggemos W, Seilmaier M, Zange S, Müller MA, et al. Virological assessment of hospitalized patients with COVID-2019. *Nature*. 2020;581(7809):465–469.
- [39] Lauer SA, Grantz KH, Bi Q, Jones FK, Zheng Q, Meredith HR, et al. The incubation period of coronavirus disease 2019 (COVID-19) from publicly reported confirmed cases: estimation and application. *Annals of Internal Medicine*.

2020;172(9):577–582.

- [40] Danchin M, Koirala A, Russell F, Britton P. Is it more infectious? Is it spreading in schools? This is what we know about the Delta variant and kids; 2021. Accessed on 10 July 2021. <https://theconversation.com/is-it-more-infectious-is-it-spreading-in-schools-this-is-what-we-know-about-the-delta-variant-and-kids-163724>.
- [41] Health Protection NSW. COVID-19 (Coronavirus) statistics. 28 June 2021; 2021. Accessed on 10 July 2021. https://www.health.nsw.gov.au/news/Pages/20210628_00.aspx.
- [42] Bernal JL, Andrews N, Gower C, Gallagher E, Simmons R, Thelwall S, et al. Effectiveness of COVID-19 vaccines against the B.1.617.2 variant. medRxiv. 2021.
- [43] Harris RJ, Hall JA, Zaidi A, Andrews NJ, Dunbar JK, Dabrera G. Impact of vaccination on household transmission of SARS-CoV-2 in England. medRxiv. 2021.

Supplementary Material

Model calibration

The model calibration varied the scaling factor κ (which scales age-dependent contact and transmission rates) in increments of 0.1. The best matching κ was identified when the resultant reproductive number, estimated in this work using age-stratified weights²⁵, was close to $R_0 = 6.0$. The procedure resulted in the following parametrisation:

- the scaling factor $\kappa = 5.3$ produced $R_0 = 5.97$ with 95% CI of 5.93–6.00 ($N = 6318$, randomly re-sampled in 100 groups of 100 samples; confidence intervals constructed by bootstrapping with the bias-corrected percentile method³²);
- the fraction of symptomatic cases was set as $\sigma_a = 0.67$ for adults, and $1/5$ of that, i.e., $\sigma_c = 0.134$, for children;
- different transmission probabilities for asymptomatic/presymptomatic and symptomatic agents were set as “asymptomatic infectivity” (factor of 0.5) and “pre-symptomatic infectivity” (factor of 1.0)^{33,34};
- incubation period T_{inc} was chosen to follow log-normally distributed incubation times with mean 4.4 days ($\mu = 1.396$ and $\sigma = 0.413$)³⁵;
- a post-incubation infectious asymptomatic or symptomatic period was set to last between 7 and 14 days (uniformly distributed)^{36,37,38}; and
- different detection probabilities were set as symptomatic (detection per day is 0.23) and asymptomatic/pre-symptomatic (detection per day is 0.01)¹⁶.

Sensitivity analysis

Several internal parameters have been varied during prior sensitivity analyses^{1,16}. For this study, we carried out additional sensitivity analyses in terms of the incubation period, the reproductive number, the generation period, and the fraction of symptomatic cases for children σ_c . The analysis presented below covers the time period between 17 June and 13 July inclusively, and is based on the pre-pandemic vaccination rollout. It can be contrasted with the progressive vaccination rollout studied in the main manuscript.

Incubation period. While previously the incubation period of COVID-19 was estimated to be distributed with the mean 5.5 days^{33,39}, a more recent study of the Delta variant reported a shorter mean incubation period: 4.4 days (with 95% CI of 3.9-5.0)³⁵. Our previous sensitivity analysis¹ showed that the

model is robust to changes in the time to peak infectivity, investigated in the range between 4 and 7 days. Here we investigated the sensitivity of the updated model to changes in the incubation period specifically, varying it between the mean 4.4 days (log-normally distributed with $\mu = 1.396$ and $\sigma = 0.413$), matching the estimates of Zhang et al.³⁵ and the mean 5.5 days (log-normally distributed with $\mu = 1.644$, $\sigma = 0.363$)³³.

The comparison between the 4.4-day and 5.5-day incubation periods was carried out for the same scaling factor $\kappa = 5.3$. The corresponding reproductive number changed from $R_0 = 5.97$ (95% CI of 5.93–6.00, $N = 6318$, $T_{inc} = 4.4$) to $R_0 = 6.39$ (95% CI of 6.36–6.43, $N = 7804$, $T_{inc} = 5.5$), that is, by approximately 7%. Similarly, the corresponding generation periods changed from $T_{gen} = 6.88$ (95% CI of 6.81–6.94, $N = 6318$, $T_{inc} = 4.4$) to $T_{gen} = 7.77$ (95% CI of 7.71–7.83, $N = 7804$, $T_{inc} = 5.5$), i.e., by approximately 13%. This relatively small sensitivity is explained by the high level of infectivity exhibited in our model by pre-symptomatic and asymptomatic individuals, see. Fig. S1.

Sensitivity of nowcasting outcomes. Furthermore, using the suppression threshold of 100 cases, corresponding to the initial restrictions (June 27), we contrasted the nowcasting scenarios based on different incubation periods. In doing so, we also varied global scalars κ producing different reproductive numbers and generation periods, thus extending the sensitivity analysis beyond local sensitivities. Specifically, for $T_{inc} = 5.5$, the scaling factor $\kappa = 5.0$ produced the reproductive number $R_0 = 6.09$ with 95% CI of 6.03–6.15 ($N = 6703$), and the generation period $T_{gen} = 7.74$ with 95% CI of 7.68–7.81. For each setting, we identified the levels of social distancing (SD), triggered by the suppression threshold of 100 cases (June 27), that best matched the actual incidence data. This comparison allowed us to establish robustness of the model outcomes to changes in T_{inc} , R_0 and T_{gen} . The outcomes are shown in Fig. S2 ($T_{inc} = 4.4$ and $R_0 = 5.97$, $T_{gen} = 6.88$, produced by $\kappa = 5.3$) and Fig. S3 ($T_{inc} = 5.5$ and $R_0 = 6.09$, $T_{gen} = 7.74$, produced by $\kappa = 5.0$).

The SD levels were based on moderately reduced interaction strengths detailed in Table 1. For the setting with shorter incubation period, the best matching nowcasting scenario was given by $SD = 0.5$, see Fig. S2, with growth rate $\beta_{0.4} = 0.093$ being the closest match to the actual growth rate $\beta_I = 0.098$. For the setting with longer incubation period, the best matching nowcasting scenario was produced by $SD = 0.4$, see Fig. S3, with $\beta_{0.3} = 0.099$ being the closest match to β_I , while $\beta_{0.4} = 0.084$ was within the range. The sensitivity analysis revealed that the nowcasting model outcomes are not strongly influenced by changes in T_{inc} , R_0 and T_{gen} within the explored ranges. In other words, it confirmed the conclusion that the social distancing compliance, at least until July 13, has been followed only moderately (around $SD = 0.4$), and would be inadequate to suppress the outbreak.

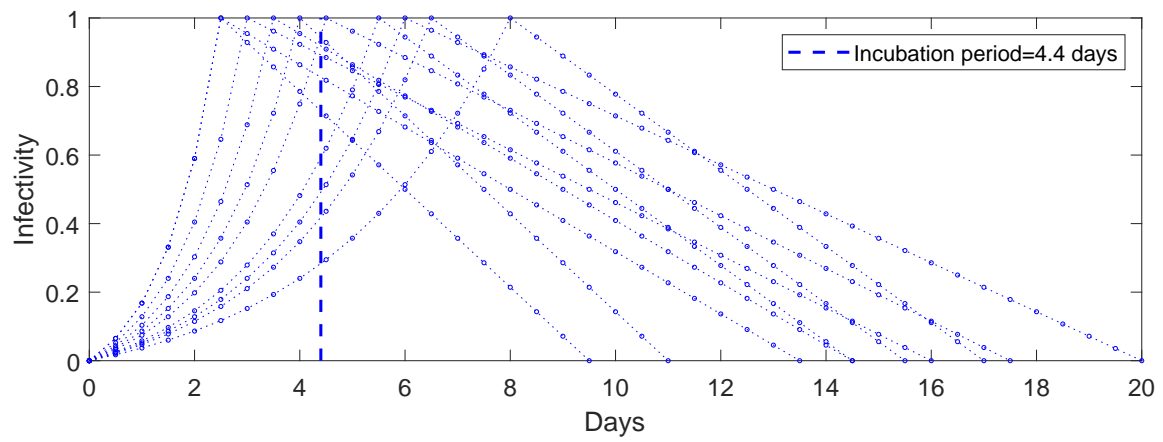
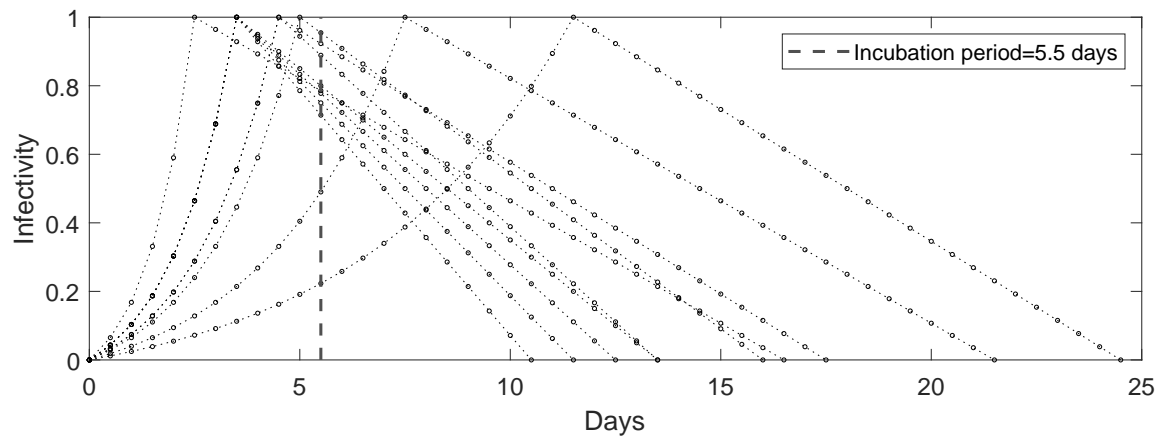


Figure S1: Model of the natural history of COVID-19. Profiles of the infectivity are sampled from 20 random agents, with each profile rising exponentially until a peak, followed by a linear decrease to full recovery. Vertical dashed lines indicate the mean incubation period T_{inc} : 5.5 days (top) and 4.4 days (bottom), with the means distributed log-normally.

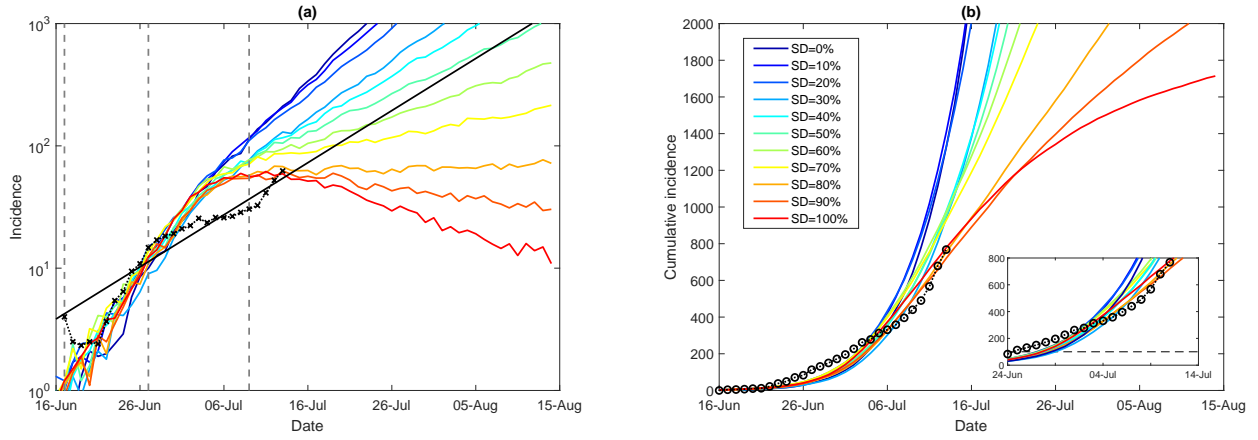


Figure S2: **Nowcasting up to July 13 (pre-pandemic vaccination rollout; suppression threshold: 100 cases): a comparison between actual epidemic curves and nowcasting simulation scenarios** ($T_{inc} = 4.4$, $R_0 = 5.97$, $T_{gen} = 6.88$). A moving average of the actual time series for (a) (log-scale) incidence (crosses), and (b) cumulative incidence (circles); with an exponential fit of the incidence's moving average (black solid). Vertical dashed marks align the simulated days with the outbreak start (17 June, day 11), initial restrictions (27 June, day 21), and tighter lockdown (9 July, day 33). Traces corresponding to each social distancing (SD) compliance level are shown as average over 10 runs (coloured profiles for SD varying in increments of 10%, i.e., between $SD = 0.0$ and $SD = 1.0$). Each SD strategy, coupled with school closures, begins with the start of initial restrictions, when cumulative incidence exceeds 100 cases (b: inset). The alignment between simulated days and actual dates may slightly differ across separate runs. Case isolation and home quarantine are in place from the outset.

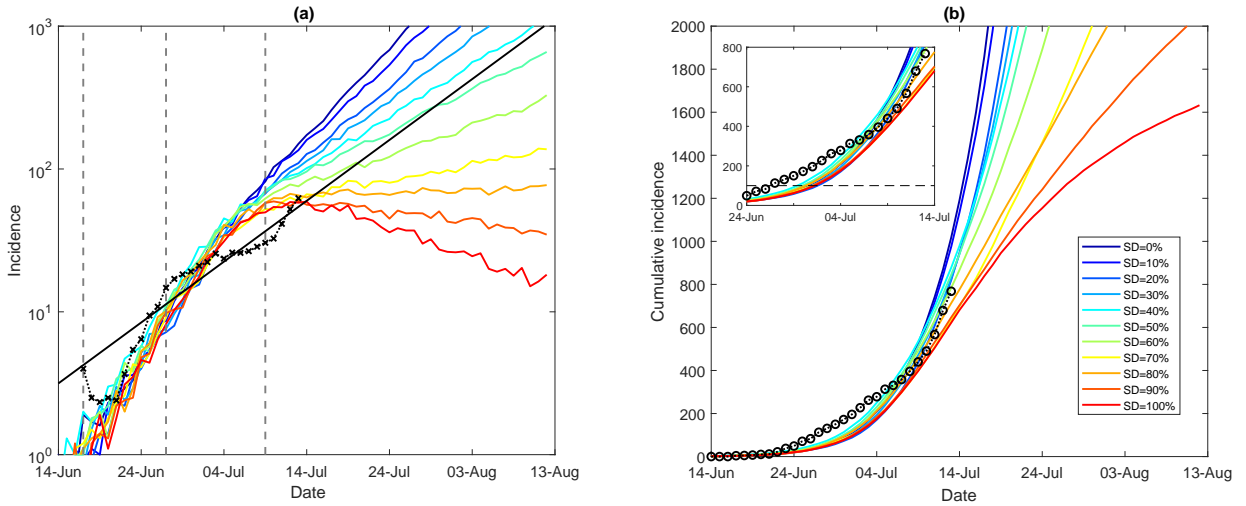


Figure S3: **Nowcasting up to July 13 (pre-pandemic vaccination rollout; suppression threshold: 100 cases): a comparison between actual epidemic curves and nowcasting simulation scenarios** ($T_{inc} = 5.5$, $R_0 = 6.09$, $T_{gen} = 7.74$). A moving average of the actual time series for (a) (log-scale) incidence (crosses), and (b) cumulative incidence (circles); with an exponential fit of the incidence's moving average (black solid). Vertical dashed marks align the simulated days with the outbreak start (17 June, day 13), initial restrictions (27 June, day 23), and tighter lockdown (9 July, day 35). Traces corresponding to each social distancing (SD) compliance level are shown as average over 10 runs (coloured profiles for SD varying in increments of 10%, i.e., between $SD = 0.0$ and $SD = 1.0$). Each SD strategy, coupled with school closures, begins with the start of initial restrictions, when cumulative incidence exceeds 100 cases (b: inset). The alignment between simulated days and actual dates may slightly differ across separate runs. Case isolation and home quarantine are in place from the outset.

Sensitivity of suppression outcomes. We also contrasted the suppression scenarios based on different incubation periods, reproductive numbers and generation periods (again using the threshold of 100 cases, triggered by the initial restrictions imposed on June 27). We explored feasible SD levels, $0.5 \leq SD \leq 0.9$, staying with $CI = 0.7$ and $HQ = 0.5$, but using the lowest feasible interaction strengths ($NPI_c = 0.1$, where NPI is one of CI, HQ, SC and SD), as specified in Table 1. For each setting, we identified the duration of suppression measures required to reduce the incidence below 10. The results are shown in Fig. S4 ($T_{inc} = 4.4$, $R_0 = 5.97$, $T_{gen} = 6.88$, $\kappa = 5.3$) and Fig. S5 ($T_{inc} = 5.5$, $R_0 = 6.09$, $T_{gen} = 7.74$, $\kappa = 5.0$).

For each setting, a suppression of the outbreak is observed only for macro-distancing at $SD \geq 0.7$. Specifically, at $SD = 0.8$, new cases reduce below 10 per day approximately a month after a peak in incidence (when $T_{inc} = 5.5$, $R_0 = 6.09$), and the alternate setting ($T_{inc} = 4.4$, $R_0 = 5.97$) achieves this target a few days earlier (in 28 days). At $SD = 0.7$ the difference between the settings grows: while for the setting with $T_{inc} = 5.5$, $R_0 = 6.09$ the post-peak suppression period exceeds two months, the alternative ($T_{inc} = 4.4$, $R_0 = 5.97$) approaches the target about eight weeks (55 days) after the peak. There is a minor difference between the considered settings at $SD = 0.9$ which would achieve the required reduction within three weeks following the peak in incidence. The sensitivity analysis shows that changes in T_{inc} , R_0 and T_{gen} within the considered ranges do not strongly affect the modelled suppression outcomes. This supports the projection that the peak in incidence would be followed by approximately four weeks at $SD = 0.8$, and that this period would lengthen at least twice if the compliance reduced by 10% to $SD = 0.7$ (this setting produced the highest sensitivity among the levels demonstrating the suppression, due to its low rate of the incidence decline).

Fraction of symptomatic cases for children. There is a lack of data on the severity of COVID-19 in children, when the disease is associated with the Delta variant. During the current outbreak in Sydney, several COVID-19 cases have been reported in schools and early childhood centres, with one outbreak in a primary school at the end of June involving four children^{40,41}. Nevertheless, we analysed the model sensitivity to changes in the fraction of symptomatic cases for children, varying it from $\sigma_c = 0.134$ to a higher value ($\sigma_c = 0.268$). This analysis was carried out for the incubation period $T_{inc} = 4.4$ days and the scalar $\kappa = 5.3$.

The reproductive number increased from $R_0 = 5.97$ for the lower fraction (95% CI of 5.93–6.00, over $N = 6318$ simulations), to $R_0 = 6.20$ for the higher fraction (with 95% CI of 6.16–6.23, $N = 6609$). The change was within 4%. The generation period has changed even less: from $T_{gen} = 6.88$ for the lower fraction (95% CI of 6.81–6.94, $N = 6318$), to $T_{gen} = 6.93$ (with 95% CI of 6.87–6.99, $N = 6609$). This change

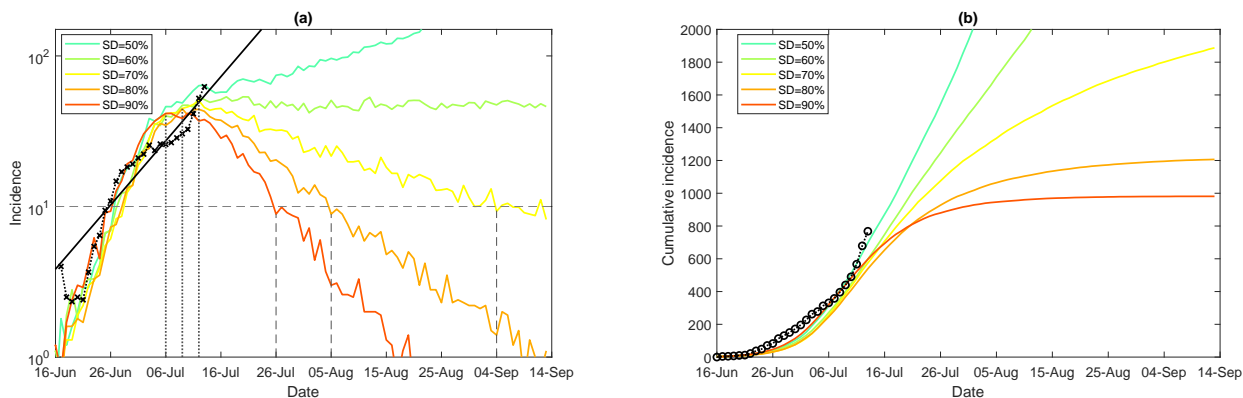


Figure S4: **Suppression after June 27 (pre-pandemic vaccination rollout; suppression threshold: 100 cases): a comparison between actual epidemic curves and counter-factual simulation scenarios** ($T_{inc} = 4.4$, $R_0 = 5.97$, $T_{gen} = 6.88$). A moving average of the actual time series for (a) (log scale) incidence (crosses), and (b) cumulative incidence (circles). Traces corresponding to feasible social distancing (SD) compliance level are shown as average over 10 runs (coloured profiles for SD varying in increments of 10%, i.e., between $SD = 0.5$ and $SD = 0.9$). Vertical lines mark the incidence peaks (dotted) and reductions below 10 daily cases (dashed). Each SD strategy, coupled with school closures, begins with the start of initial restrictions (i.e., 27 June, simulated day 21), when cumulative incidence exceeds 100 cases. The alignment between simulated days and actual dates may slightly differ across separate runs. Case isolation and home quarantine are in place from the outset.

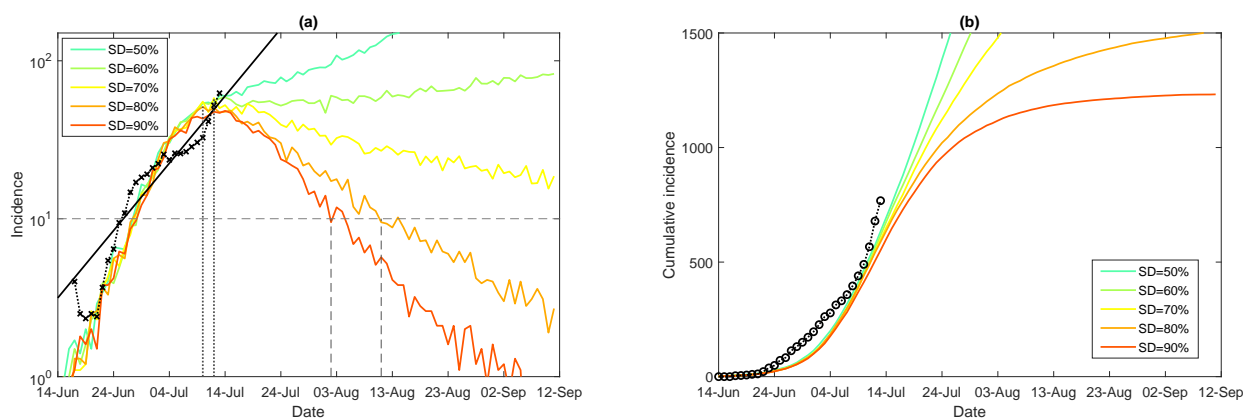


Figure S5: **Suppression after June 27 (pre-pandemic vaccination rollout; suppression threshold: 100 cases): a comparison between actual epidemic curves and counter-factual simulation scenarios** ($T_{inc} = 5.5$, $R_0 = 6.09$, $T_{gen} = 7.74$). A moving average of the actual time series for (a) (log scale) incidence (crosses), and (b) cumulative incidence (circles). Traces corresponding to feasible social distancing (SD) compliance level are shown as average over 10 runs (coloured profiles for SD varying in increments of 10%, i.e., between $SD = 0.5$ and $SD = 0.9$). Each SD strategy, coupled with school closures, begins with the start of initial restrictions (i.e., 27 June, simulated day 23), when cumulative incidence exceeds 100 cases. The alignment between simulated days and actual dates may slightly differ across separate runs. Case isolation and home quarantine are in place from the outset.

stayed within 1%, with confidence intervals overlapping. Such low sensitivity is in agreement with our prior analysis showing slow linear increases of R_0 and T_{gen} in response to changes in the fraction σ_c ¹.

Vaccination modelling

The national COVID-19 vaccine rollout strategy pursued by the Australian Government follows a hybrid approach combining two vaccines: BNT162b2 (Pfizer/BioNTech) and ChAdOx1 nCoV-19 (Oxford/AstraZeneca), administered across specific age groups, e.g., the Australians younger than 60 are generally eligible for the BNT162b2 vaccine. Our model accounts for differences in vaccine efficacy for the two vaccines approved for distribution in Australia, and distinguishes between separate vaccine components: efficacy against susceptibility (VEs), disease (VEd) and infectiousness (VEi).

For the pre-pandemic vaccination rollout, the extent of pre-outbreak vaccination coverage was set at 6% of the population, matching the level actually achieved in Australia by mid-June 2021. For the progressive vaccination rollout, the initial coverage was set at zero, followed by vaccination uptake averaging 3% per week for the duration of simulation, reaching approximately 9% by the end of June (cf., 7.92% of the actual vaccination coverage¹⁴), 15% by mid-July, 27% by mid-August, and approaches 40% by mid-September.

In setting the efficacy of vaccines against B.1.617.2 (Delta) variant, we followed the study of Bernal et al.⁴² which estimated the efficacy of BNT162b2 (Pfizer/BioNTech) as $VEc \approx 0.9$ (more precisely, 87.9% with 95% CI: 78.2 to 93.2), and the efficacy of ChAdOx1 nCoV-19 (Oxford/AstraZeneca) as $VEc \approx 0.6$ (i.e., 59.8% with 95% CI: 28.9 to 77.3). Given the constraint for the clinical efficacy¹⁶:

$$VEc = VEd + VEs - VEs VEd, \tag{S1}$$

we set $VEd = VEs = 0.684$ for BNT162b2, and $VEd = VEs = 0.368$ for ChAdOx1 nCoV-19.

Recent studies also provided the estimates of efficacy against infectiousness (VEi) for both considered vaccines at a level around 0.5⁴³. A general sensitivity analysis of the model to changes in VEi and VEc was carried out in¹⁶.

In both rollout scenarios, the vaccinations are assumed to be equally balanced between the two vaccines, so that each type is given to approximately (i) 0.7M individuals initially, by mid-June, or (ii) 4.7M individuals progressively, by mid-September. Vaccines are distributed according to specific age-dependent allocation ratios, $\approx 2.457:30:1$, mapped to age groups $[\text{age} \geq 65] : [18 \leq \text{age} < 65] : [\text{age} < 18]$, as explained in our prior work¹⁶.

Table S1: The growth rate of the observed incidence.

growth rate	period	mean	95% CI
β_I	17 June – 13 July	0.098	0.084–0.112
β_{II}	17 June – 25 July	0.076	0.069–0.084
β_{III}	16 July – 25 July	0.037	0.026–0.048

Growth rates

To estimate growth rates β , we fit a 7-day moving average of the corresponding incidence time series $I(t)$ to an exponential function $\alpha \exp(\beta(t))$, using MATLAB R2020a function `movmean(I, [6 0])`. The growth rate of the observed incidence were estimated for several time periods (see Table S1).

The growth rates β_{SD} for the time series simulated for each SD level between 0.0 and 1.0 were estimated for the periods lasting from either the start of initial restrictions (27 June), or from 16 July (comprehensive lockdown measures were announced on 17 July), until the end of simulation.